Comparative Coordination Chemistry of PNP and SNS Pincer Ruthenium Complexes

Danielle N. Chirdon,[a] Steven P. Kelley,[a] Nilay Hazari[b] and Wesley H. Bernskoetter[a,*]

[a] The Department of Chemistry, The University of Missouri, Columbia, Missouri, 65211, USA.
E-mail: bernskoetterwh@missouri.edu

[b] The Department of Chemistry, Yale University, P. O. Box 208107, New Haven, Connecticut, 06520, USA.

Abstract

Ruthenium carbonyl complexes supported by PNP pincer ligands are prominent catalysts for a range of hydrogenation and dehydrogenation reactions. Recently, Ru complexes with cheaper, more air stable SNS pincer ligands have emerged as attractive alternatives for the development of improved catalysts. However, there is currently a paucity of information on how the replacement of the phosphine donors in PNP ligands with the sulfur donors in SNS ligands influences the synthesis, structure and electronic properties of the resulting metal complexes. Herein, the coordination chemistry of a series of Ru carbonyl complexes with SNS pincer ligands has been systematically compared with related PNP-ligated species. Three different SNS pincer ligands were explored including a pyridyl based $NC_5H_3\{CH_2(S^tBu)\}_2$ ligand and two aliphatic ligands, $HN\{CH_2CH_2(S^tBu)\}_2$ and $NCH_3\{CH_2CH_2(S^tBu)\}_2$, along with different combinations of monodentate ancillary ligands. The geometric structures of the SNS and PNP Ru complexes were studied using NMR spectroscopy and X-ray crystallography. Additionally, the redox properties and electronic structures of these complexes were probed through a combination of cyclic voltammetry and DFT calculations. Overall, differences between SNS and PNP complexes extend well beyond simply modulating inductive donation to the metal and include changes in synthetic outcomes, as well as variations in geometry that impact redox behavior. Our study reveals fundamental information about the coordination chemistry of the SNS ligand, which may aid in interpreting catalytic results.

Introduction

Ru complexes supported by PNP pincer ligands have facilitated remarkable advances in the reversible, catalytic hydrogenation of polar substrates.[1,2] For example, several variants of complexes related to Ru-MACHO [Ru(^{R}PN^{H}P)(CO)(Cl)(H)] (^{R}PN^{H}P= HN{$CH_2CH_2(PR_2)$}$_2$) (**1**, Figure 1), which contains a PNP ligand with a flexible aliphatic linker, are excellent catalysts for dehydrogenative transformations such as methanol oxidation[3] and acceptorless dehydrogenative coupling (ADC) of alcohols to esters.[4] In many cases, variants of **1** are also leading catalysts for the microscopic reverse hydrogenation reactions. For instance, these species are effective catalysts for the hydrogenation of CO_2 to methanol[5] and are utilized industrially in the hydrogenation of esters to alcohols.[6] Likewise, Ru catalysts supported by pyridine-based PNP ligands (Milstein catalysts) (**2**, Figure 1) excel at the interconversion of CO_2 and H_2 with formate,[7] as well as the hydrogenation of a plethora of substrates ranging from nitriles to amides.[8]

Mechanistic studies probing the outstanding activity of PNP supported Ru catalysts have attributed their success to several key features of the ligand. These include the improved catalyst stability engendered by tridentate pincer binding and the ability of the ligand to participate in metal ligand cooperativity either through aromatization/dearomatization in pyridyl PNP ligands[9] or through deprotonation and hydrogen bonding in their aliphatic counterparts.[3,10] A recent report by Prakash and coworkers has also highlighted the importance of electron donation from the pincer ligand in catalyst performance. While studying a series of aliphatic PNP Ru catalysts, it was observed that those species bearing less electron donating ligands provided greater turnover for CO_2 hydrogenation to methanol. Prakash *et al.* hypothesized that more electron poor PNP Ru species engage in weaker π-backbonding, which destabilizes an inactive Ru dicarbonyl species, [Ru(^{R}PN^{H}P)$(CO)_2$(H)]$^+$ (**3**), (Figure 1) allowing it to re-enter the catalytic cycle.[11] A logical extension of this hypothesis is to change the heteroatom donors in the pincer ligand to generate improved catalysts that contain metal centers that are less electron rich.

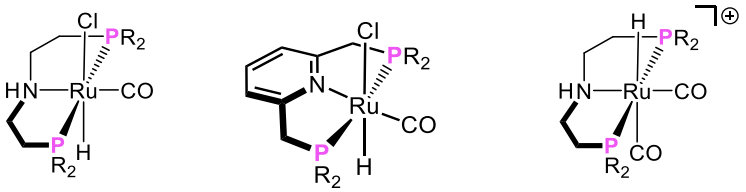

Figure 1. Selected ^{R}PNP Ru complexes relevant to catalytic (de)hydrogenation.

The replacement of PNP pincer ligands with SNS ligands that contain more weakly σ-donating thioether groups in place of the phosphine donors may be a useful approach to lowering the electron density at the metal. In fact, SNS pincer ligands have already been used to support base metal[12,13] and palladium[14,15] catalysts due to their relative air stability, facile synthesis and potential hemilability compared to the PNP ligand platform. For example, palladium catalysts with either pyridyl or aliphatic SNS ligands can facilitate cross-coupling reactions that are proposed to involve homogeneous**Error! Bookmark not defined.** or heterogeneous**Error! Bookmark not defined.** active species. Further, the aliphatic SNS complex [Cr(^{Et}SN^{H}S)(Cl)$_3$] (^{Et}SN^{H}S= HN{CH$_2$CH$_2$S(Et)}$_2$) gives the same high activity and selectivity for ethylene trimerization as PNP supported Cr(III) catalysts, but with lower cost, toxicity, and air sensitivity.[16]

Following these catalytic successes, extensive efforts have also been made to use highly practical SNS ligands as replacements for the quintessential PNP pincer ligands in Ru hydrogenation catalysts. Initial work employed pyridyl SNS Ru complexes typified by [Ru(^{tBu}SN$_{py}$S)(MeCN)(Cl)$_2$] (**4**) and [Ru(^{tBu}SN$_{py}$S)(PPh$_3$)(Cl)$_2$] (**5-PPh$_3$**) (^{tBu}SN$_{py}$S= NC$_5$H$_3${CH$_2$S(tBu)}$_2$) (Figure 2), which are effective catalysts for the transfer hydrogenation of acetophenone.[17] Subsequently, Gusev and coworkers reported an aliphatic SNS Ru complex, [Ru(^{Et}SN^{H}S)(PPh$_3$)(Cl)$_2$] (**6**) (Figure 2), which outperforms popular PNN and PNP congeners, including **1**, in select ester hydrogenation reactions, as well as the ADC of alcohols.[18] Although catalyst **1** ultimately remains superior to **6** for the reduction of CO$_2$,[5b,19] the aliphatic SNS Ru species has proven competitive with PNP Ru analogs for several catalytic transformations including ester metathesis, transfer hydrogenation, and cyclopropanation,[20] Most recently, **6** has also compared favorably with PNP congeners in the selective hydrogenation of long chain aliphatic nitriles to amines.[21]

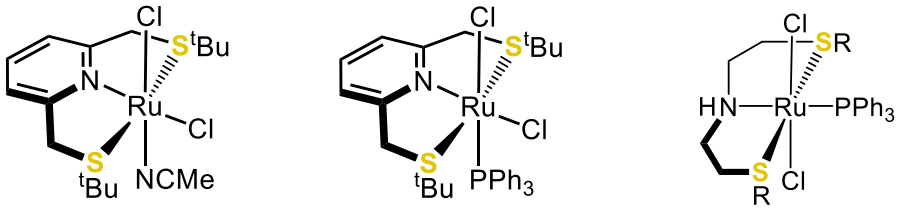

4 **5-PPh$_3$** **6** (R= Et) **7-PPh$_3$** (R= ^{t}Bu)

Figure 2. Structures of SNS Ru complexes previously investigated for catalysis including Gusev's aliphatic SNS catalyst **6** (right) and pyridyl SNS Ru complexes tested for transfer hydrogenation (left, **4** and **5-PPh$_3$**).

While the multitude of comparative catalytic results provide intriguing information about the impact of the SNS pincer ligand on performance, the underlying impact of SNS ligands on the structural and electronic properties of the resulting complexes have not been widely explored. For (de)hydrogenative catalysis, understanding the impact of the pincer ligand on metal electron density may be particularly important as this feature is key to the stability of a common deactivation complex, the metal dicarbonyl species (*vida supra*).[11] Metal electron richness also likely controls the ease of elementary steps in catalysis such as hydride insertion,[22] oxidative addition, or reductive elimination.[23] This work seeks to uncover electronic and other fundamental influences of SNS pincer ligands by comparing X-ray crystal structures, electrochemistry, and calculated structures for a family of dichloro SNS Ru complexes and their direct PNP analogs. Beyond altering the pincer heteroatoms, the pincer backbone (Figure 3) and ancillary ligands were also systematically modified to explore their effects. Carbonyl ancillary ligands have drawn our particular focus due to their prevalence in leading PNP catalyst structures. However, to this point, few SNS carbonyl complexes have been reported. Previous studies of SNS Ru families use PPh_3 or DMSO as the neutral ancillary ligand,[24,25] and empirical catalytic studies tend to compare PNP carbonyl complex **1** with SNS precatlayst **6** which bears a PPh_3 instead of CO ligand. Herein, we describe the preparation and properties of several new SNS Ru carbonyl complexes. Direct comparisons of the SNS Ru compounds and their more established PNP analogs reveal intertwined structural and electronic effects from ligand modifications providing guidance for the role of ligand influence in catalytic performance.

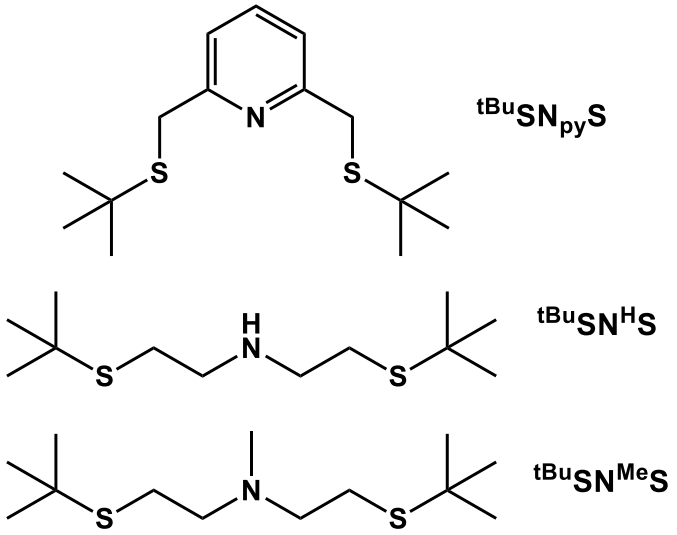

Figure 3. SNS ligands used for comparative coordination chemistry studies.

Results and Disucssion

Synthesis of SNS Ru Complexes

The SNS ligands used in this study (Figure 3) are all air stable and feature a t-butyl substituent on each sulfur donor to provide steric protection at the metal and a characteristic resonance for ^{1}H NMR spectroscopy. The ligand backbones investigated reflect the pincer ligands commonly used in Ru (de)hydrogenation catalysis[1,2,10b] and include a pyridyl version, as well as aliphatic structures with either a secondary or tertiary amine. The ligands ^{tBu}**SN^{H}S** and ^{tBu}**SN$_{py}$S** were both synthesized in one step using the method described by Waser ,which involves the substitution of an organohalide with t-butyl thiol.[25] The ^{tBu}**SN^{Me}S** ligand was prepared from ^{tBu}**SN^{H}S** via Eschweiler–Clarke methylation of the amine, as previously described for a similar derivative by Gusev.[18] In our hands, neat oils of ^{tBu}**SN^{H}S** began degrading over a day at ambient temperatures, but long-term storage was possible at low temperatures in dilute pentane solutions.

For the more widely studied PNP Ru systems, pincer-ligated carbonyl species can be readily obtained through displacement of PPh_3 and dimethylformamide (DMF) from the Ru source [Ru(CO)(DMF)(PPh_3)$_2$(Cl)$_2$], which conveniently has CO preinstalled (Scheme 1).[26] However, attempts to use this route with ^{tBu}**SN^{H}S** resulted in incomplete chelation of the pincer ligand.[27] Though not isolated, the κ^2-S,N complex, [Ru(κ^2-^{tBu}**SN^{H}S**)(CO)(PPh_3)(Cl_2)] (**9**) (Scheme 1) was identified in the reaction mixture through NMR spectroscopy. Specifically, *in-*

situ ^{31}P NMR spectra show synchronous growth of peaks for a new bound phosphine (34.5 ppm) and free PPh_3 (-4.7 ppm). Further, the post reaction ^{1}H NMR spectrum exhibits two significantly shifted but equally intense S-^{t}Bu groups, one at 1.27 ppm consistent with coordinated S-^{t}Bu and one at 0.70 ppm more likely indicating unbound S-^{t}Bu (See SI, Figure S13).

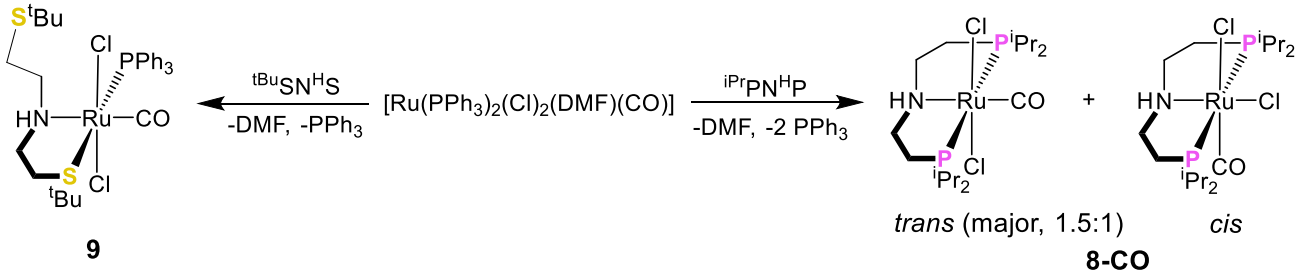

Scheme 1. Synthesis of Ru carbonyl complexes through PPh_3 displacement using aliphatic SNS (left) and PNP (right) ligands.

To avoid incomplete chelation, the desired κ^3-SNS Ru carbonyl structure was accessed through an alternative approach inspired by the ability of CO to displace DMSO ligands.[28] SNS complexes with labile DMSO were prepared as synthetic intermediates by refluxing each SNS variant with $[Ru(DMSO)_4(Cl)_2]$ (Figure 4).[24a] Formation of the SNS ligated Ru DMSO complexes **5-DMSO, 7-DMSO** and **10-DMSO** was confirmed by the presence of signals corresponding to bound DMSO between 2.66 and 3.62 ppm in the ^{1}H NMR spectra. These shifts are in agreement with those previously reported for Ru DMSO species.[24a,28,29] Additionally, infrared (IR) spectra for the SNS Ru DMSO complexes exhibit S=O stretching bands between 1045-1160 cm^{-1}, consistent with S-bound DMSO ligands.[30,31] DMSO was displaced from the intermediate complexes by adding 1 atm of CO and either heating in the case of the aliphatic SNS complexes or applying UV irradiation for the pyridyl derivative to give the desired carbonyl complexes $[Ru(^{tBu}SN^{H}S)(CO)(Cl)_2]$ (**7-CO**), $[Ru(^{tBu}SN^{Me}S)(CO)(Cl)_2]$ (**10-CO**), and $[Ru(^{tBu}SN_{py}S)(CO)(Cl)_2]$ (**5-CO**) (Figure 4). The coordination of CO to the metal was evident from the appearance of intense CO stretching vibrations in the IR spectra (Table 1). The SNS Ru dichloride carbonyl complexes were also characterized using NMR spectroscopy, elemental analysis, and where possible, X-ray crystallography (*vide infra*).

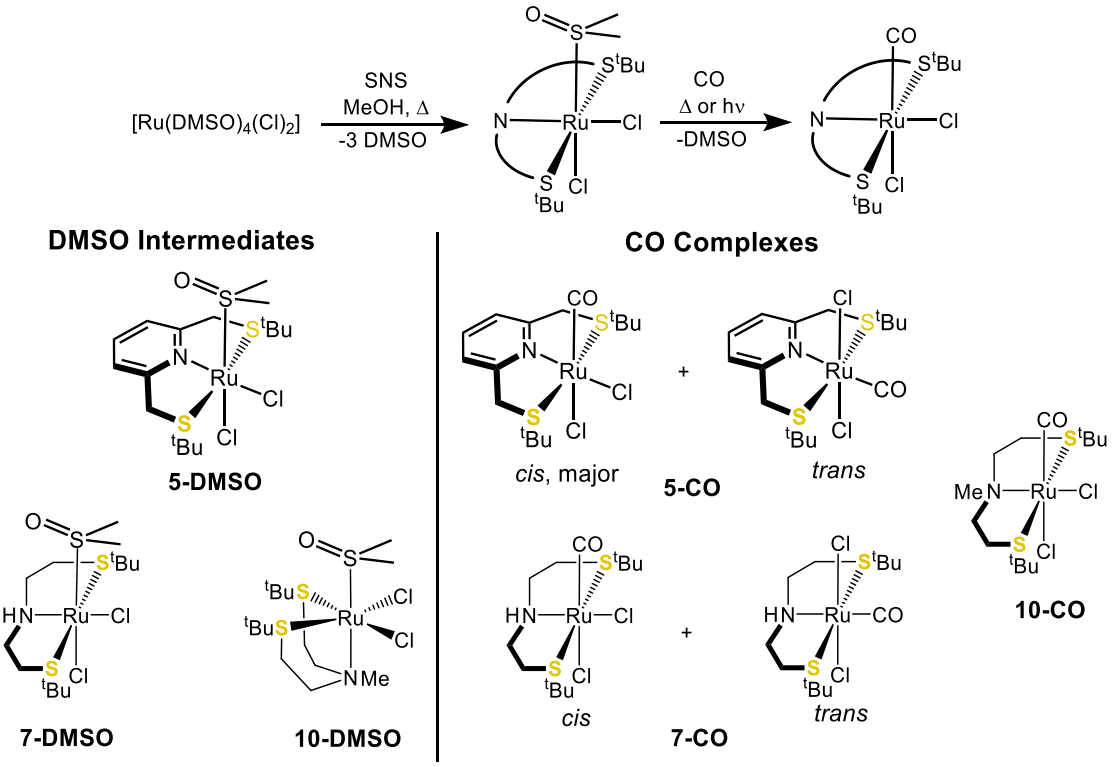

Figure 4. Synthesis of SNS Ru dichloride carbonyl complexes via intermediate Ru DMSO adducts.

In order to provide comparisons to PNP Ru dicarbonyl complexes, which are key catalyst deactivation species, dicarbonyl versions of the aliphatic and pyridyl SNS complexes were next targeted for synthesis.[11] The $^{tBu}SN_{py}S$ Ru dicarbonyl complex $[Ru(^{tBu}SN_{py}S)(CO)_2Cl][PF_6]$ (**5-2CO**), was synthesized cleanly via ligand addition to the coordination polymer $[Ru(CO)_2(Cl)_2]_n$ (Scheme 2), a method which has been used to obtain similar species containing pyridyl PNP[32] or terpyridine[33] ligands. The identity of **5-2CO** was verified by single crystal X-ray diffraction (*vide infra*) as well as the observation of two relatively high frequency carbonyl stretches at 2082 and 2031cm^{-1} in the IR spectrum (Table 1). Unfortunately, the same synthetic method proved unsuccessful for the aliphatic $^{tBu}SN^{H}S$ ligand. Likewise, silver abstraction of chloride from **7-CO** under an atmosphere of CO also failed to produce the cationic dicarbonyl species.[34] An alternate cation $[Ru(^{tBu}SN^{H}S)(MeCN)(CO)(Cl)][BF_4]$ (**7-ACN**) was however formed as a possible intermediate to the dicarbonyl species by treating **7-CO** with tritylium tetrafluoroborate in ACN (Scheme 3).[35] The formation of this cation was indicated by the ^{1}H NMR spectrum containing a singlet at 2.68 ppm corresponding to bound ACN,[36] and the IR spectra displaying the expected shift of the CO vibration from 1946 cm^{-1} in **7-CO** to 1961 cm^{-1} in **7-ACN**. The nitrile ligand in

7-ACN was ultimately displaced to give the desired dicarbonyl [Ru(^{tBu}SN^{H}S)(CO)$_2$(Cl)][BF$_4$] (**7-2CO**) by prolonged heating under CO atmosphere. Addition of the second CO ligand was confirmed by X-ray crystallography (*vide infra*) as well as IR spectroscopy, where two intense carbonyl stretches at 2072 and 2008 cm^{-1} were observed.

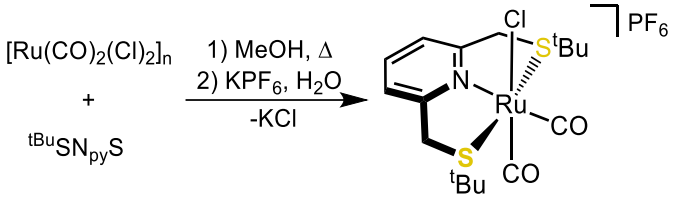

5-2CO

Scheme 2. Synthesis of cationic, dicarbonyl complex **5-2CO**.

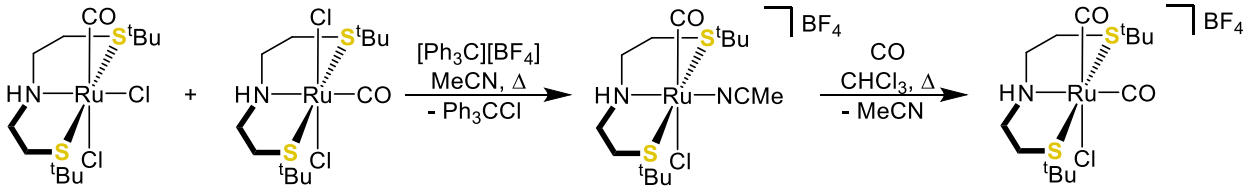

7-CO **7-ACN** **7-2CO**

Scheme 3. Synthesis of dicarbonyl **7-2CO** via intermediate cation **7-ACN**.

Structural Characterization of Pincer Ru Complexes

The novel SNS Ru complexes synthesized in this work could exist in multiple configurations which vary in the coordination mode of the pincer ligand (meridional or facial) and the arrangement of the monodentate ligands (*cis* or *trans*). Additionally, in complexes containing aliphatic SNS ligands, compounds could differ in the orientation of monodentate ligands with respect to the substituent on the nitrogen. A ligand could be either *syn* (on the same face as the substituent on the nitrogen donor) or *anti* (on the opposite face as the substituent on the nitrogen donor). Finally, any analysis of the isomers of SNS-ligated complexes is complicated by the orientation of the substituent on the sulfur donors (t-butyl, in this case). Due to the stereochemically active lone pair remaining after sulfur coordination, the substituents can be oriented either above or below the plane of a meridionally coordinated SNS ligand. To more fully understand the structures of the SNS ligated complexes prepared in this work, we utilized a combination of NMR spectroscopy, X-ray crystallography, and DFT calculations.

For the aliphatic SNS DMSO complex **7-DMSO**, ^{1}H NMR spectra show only one sharp resonance for the S-^{t}Bu groups and one signal for bound DMSO, suggesting a single isomer with non-fluxional S-^{t}Bu orientations. The spectra for **10-DMSO** are less sharp which could, among other possibilites, indicate similar isomers differentiated only by S-^{t}Bu positioning as seen in previous SNS complexes.[17] X-ray diffraction experiments conducted on crystals of **7-DMSO** and **10-DMSO** reveal that the Ru center is octahedrally coordinated in the solid state with DMSO bound through sulfur as expected for a soft Ru center (Figure 5).[31] However, the structures differ notably in the coordination geometry of the SNS ligand. The ^{tBu}SN^{H}S supported complex **7-DMSO** exhibits meridional pincer coordination with a cisoid chloride arrangement while the N-methyl congener **10-DMSO** has facial pincer coordination (Figure 5). Differing sterics at the pincer nitrogen may contribute to this variation in SNS binding. Additionally, the *mer* isomer is stabilized in **7-DMSO** by an intramolecular hydrogen bond between the chloride ligand and the SNS ligand N-H (H1···C11 = 2.248 Å).[37] The *fac* structure of **10-DMSO** also shows a weak interaction between the DMSO oxygen and methyl hydrogens from S-^{t}Bu (2.475 Å). Similar interactions have been found to influence the structure of other Ru-DMSO complexes.[29b,38] DFT calculations using an ICPM model with the dielectric constant for ACN are consistent with the isomers observed in the solid state. The *mer* isomer of **7-DMSO** is calculated to be slightly favored (0.5 kcal/mol) over the *fac*,[39] while the *fac* isomer of **10-DMSO** is favored by a more substantial 5.8 kcal/mol (Figure S23-S24). These results suggest that the geometric preferences observed in the solid state are not solely a result of crystal packing effects and likely persist in ACN solution.

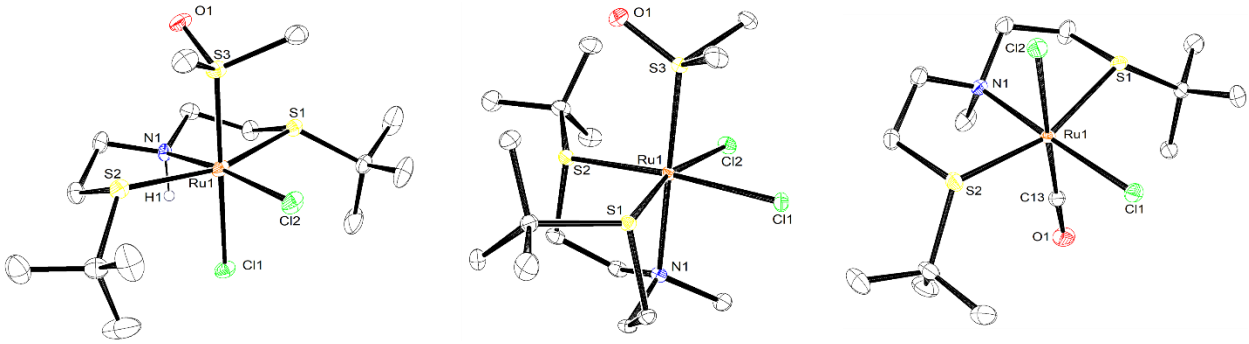

Figure 5. Solid state structures of **7-DMSO** (left), **10-DMSO** (center) and **10-CO** (right) with 30% ellipsoids. All co-crystallized solvent molecules and hydrogens not attached to heteroatoms have been omitted for clarity.

The only SNS ligated monocarbonyl species which afforded crystals suitable for X-ray diffraction experiments was **10-CO** (Figure 5). The solid state structure shows that substitution of bulky DMSO with CO results in meridional rather than facial pincer binding in **10-CO**. The chloride ligands are positioned *cis* and both S-^{t}Bu groups are positioned on the same face as the N-Me and CO ligand. DFT calculations again predict the observed solid state structure of **10-CO** to be thermodynamically favored (Figure S25). Calculations also suggest that the *trans* or *fac* isomers could be thermally accessible at ambient temperature (ΔG <0.5 kcal/mol), but spectroscopy for **10-CO** is consistent with the presence of only one isomer. The ^{1}H NMR spectrum for **10-CO** has sharp singlets for the S-^{t}Bu and N-Me protons while the IR spectrum features a single, sharp CO stretch.

Compound **8-CO** is a PN^{H}P ligated complex that closely compares to **10-CO** making its structure and electronic properties of interest. Synthesis of **8-CO** yields a mixture of two isomers with ^{31}P NMR signals at 56.4 and 46.6 ppm, suggesting *cis* and *trans* isomers of the Ru dichloride carbonyl complex (Scheme 1).[26] Separation of the isomers is possible through crystallization, and X-ray crystallography on the major isomer (δ = 56.4 ppm) shows it to have a *trans* configuration (Figure S14).[40] This observed preference for placement of halide ligands *trans* and the strong, neutral ligand opposite the pincer nitrogen dominates PNP Ru chemistry and contrasts with the *cis* halide configuration observed in **10-CO**.[41] The Ru-P bond lengths in *trans*-**8-CO** (2.328(2)-2.347(2)Å) are slightly shorter than the Ru-S bond lengths in **10-CO** (2.3544(7)-2.3580(7)Å) which are consistent with the Ru-S bond distances reported in other SNS complexes.[18a] The bond from Ru to the CO carbon, meanwhile, is notably longer in *trans*-**8-CO** (1.85(1)Å) compared to **10-CO** (1.814(2)Å) due to the stronger *trans* influence of the secondary nitrogen donor versus the chloride ligand. Despite this, IR still indicates stronger π-backbonding in *trans*-**8-CO** (ν_{CO}= 1928 cm^{-1}) relative to **10-CO** (ν_{CO}= 1944 cm^{-1}).[42]

Crystals suitable for diffraction could not be obtained for **7-CO**, so its structure was analyzed through spectroscopy and computational studies.[43] The most thermodynamically preferred isomer calculated for **7-CO** features meridional binding of the SNS ligand, with a *trans* chloride configuration and S-^{t}Bu groups positioned syn to one another (Figure S27). However, a an isomer with anti orientation of S-^{t}Bu groups is at near equal energy (ΔG < 0.1 kcal/mol), suggesting either orientations of S-^{t}Bu groups maybe accessible at room temperature. This is supported by the broadness of the S-^{t}Bu resonances associated with **7-CO** in the ^{1}H NMR

spectrum.[17] A small energy difference also separates the favored *trans* chloride isomer from an isomer with *cis* chlorides (+0.9 kcal/mol). The presence of distinct *cis* and *trans* isomers would be in agreement with the IR spectrum, which shows a distinct shoulder on the main CO stretch. Other isomers, however, are unlikely due to their high calculated energies, including those with *fac* pincer coordination (+4.6 kcal/mol) or placement of N-H anti to both S-^{t}Bu groups (+7.5 kcal/mol) which strains the chelate backbone. A distinct energy penalty (~1.2 kcal/mol) is also observed in all structures where the N-H is not on the same face as the chloride, presumably owing to loss of favorable non-covalent interactions.

A crystal structure was obtained for the dicarbonyl cation **7-2CO** and shows the two CO ligands in a *cis* arrangement (Figure 6). The pincer N-H and S-^{t}Bu groups are all positioned syn to one another pointing towards a CO ligand. Solution based DFT calculations predict that the N-H should point towards the chloride ligand to achieve a stabilizing H-bond interaction (Figure S26), but in the solid state, the N-H positioning is influenced by hydrogen bonding to the BF_4 counterion instead. DFT calculations agree with the observed *cis* arrangement of the CO ligands predicting an energy penalty of over 10 kcal/mol for *trans* CO coordination. Interestingly, *cis* CO coordination in **7-2CO** contrasts with *trans* coordination previously observed for the analogous PNP dicarbonyl complex, $[Ru(^{iPr}PN^HP)(CO)_2Cl]^+$ (**8-2CO**).[44] The bond distances from Ru to the CO carbons are noteably elongated in the PNP dicarbonyl complex (1.962(2)-1.931(1)Å) relative to the SNS complex **7-2CO** (1.892(3)-1.885(4)Å) possibly reflecting the mutual *trans* influence of the CO ligands in the PNP congener. The average C-O bond length, meanwhile, is slightly longer in **8-2CO** as compared to **7-2CO**, suggesting less backbonding in the SNS dicarbonyl cation.

Unlike the aliphatic SNS complexes discussed above, the geometry of compounds containing a pyridyl SNS ligand can be determined based on the ^{1}H NMR signals associated with the pincer methylene arms. The two protons on each methylene point towards opposite faces of the complex, resulting in two doublets for which the difference in chemical shifts reflects the disparity of the two faces. As first described by Teixidor and co-workers, asymmetric *cis* complexes are marked by higher peak separations (typically near 1 ppm) while a separation less than *ca.* 0.25 ppm denotes *trans* complexes having symmetry broken only by the direction of the sulfur substituents.[24a] Accordingly, **5-DMSO** with methylene peak separation of 1.53 ppm can be assigned as a *cis* isomer with sterics factors likely relegating the DMSO and S-^{t}Bu groups to

opposite sides. **5-CO**, meanwhile, is a mixture of a major *cis* and minor *trans* isomer represented by two sets of doublets with separation of 0.62 ppm and 0.18 ppm, respectively. Dicarbonyl complex **5-2CO** was characterized by X-ray crystallography revealing an asymmetric complex with a *cis* orientation of CO ligands and S-^{t}Bu groups syn to the chloride ligand. The crystal structure shown in Figure 6 is marked by bending of the pincer pyridyl ring pushing one of the methylene arms outside of the plane of coordination, a common characteristic of pyridyl SNS metal complexes.[17,24a]

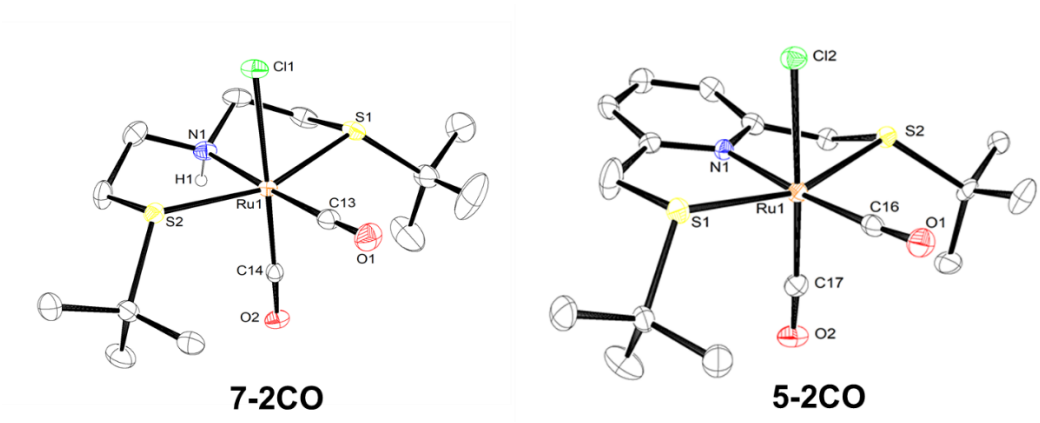

Figure 6. Solid state structures of dicarbonyl cations **7-2CO** (left) and **5-2CO** (right) at 30% ellipsoids. The counterions, cocrystallized solvent, and most hydrogens have been omitted for clarity.

Impacts of Ligand Modification on Electrochemistry

Cyclic voltammetry (CV) experiments were conducted in ACN to probe the redox properties of the SNS Ru carbonyl complexes described above. For comparison purposes, voltammograms were also collected for the PNP complex **8-CO** as well as previously described **5-PPh$_3$** [17,25] and **7-PPh$_3$**.[25] Electrochemical results are summarized in Table 1 and Figure 7. Within the explored electrochemical window (+0.76/-2.90 V), the prototypical complex **7-CO** has one major, irreversible reduction at -2.41V with a small, associated re-oxidation at -0.63 V.[45] Current for the reduction shows linear scan rate dependence indicative of diffusion control, while bulk electrolysis assigns the process as a one electron couple (Figure S15). DFT computations for the key *cis* and *trans* geometries of **7-CO** (*vide supra*)[46] suggest that reduction is best described as a Ru(II/I) redox couple. The reduction takes place at a LUMO heavily centered on the metal with significant antibonding character between the metal and p orbitals on chloride, as well as sulfur (Figure 8). This antibonding character suggests the irreversible redox behavior

likely stems from chloride loss which often accompanies reduction in chloro transition metal complexes.[47,48]

The major cathodic process and the corresponding LUMO described for **7-CO** are largely mirrored across all investigated Ru complexes with aliphatic SNS and even PNP pincer ligands (Figure 7, Figure S29). However, the phosphine containing species **7-PPh$_3$** and **8-CO** also display a reversible oxidation. This process can be assigned to the Ru^{III}/Ru^{II} couple based on the computed HOMOs (Figure S30-S31). The other complexes with aliphatic pincers show similar HOMOs, but their metal oxidation is likely just outside the observable solvent window.

Table 1: Electrochemical Properties and Carbonyl Stretches for Ru(II) SNS Complexes

Compound	Oxidation[a] $E_{1/2}$/V (ΔE/mV)	Reduction[a] E_{pc}/V	ν(CO) cm^{-1}
cis-**8-CO**	0.55 (105)	-2.71	1931
trans-**8-CO**	0.53 (78)	-2.51	1928
5-PPh$_3$	0.67[b]	-2.17, -2.70	
5-CO		-2.13, -2.86	1964
5-2CO		-1.47	2082, 2031
7-PPh$_3$	0.05 (81)	-2.63	
7-CO		-2.41	1946, 1923*sh*
7-ACN		-2.00	1961
7-2CO		-1.58	2072, 2008
10-CO		-2.27	1944

[a] Redox processes were measured under an argon atmosphere in 0.1M $TBAPF_6$/ACN using a glassy carbon working electrode scanned at 100mV/s. Potentials are reported in V vs Fc. [b]Irreversible process which is not fully observed due to the edge of the solvent window.

Potentials for the irreversible reductions vary widely across the series of aliphatic SNS and PNP pincer complexes (Table 1). Differences in ligand donor ability are implicit in this, but the impacts of geometry are also significant. Previous literature has investigated the effect of isomers on voltammetry[49] and here **8-CO**, with its separable isomers,[40] clearly demonstrates the non-trivial impact of *cis* and *trans* configurations. Comparison of pure *trans*-**8-CO** to a mixture dominated by *cis*-**8-CO** (Figure S16) reveals that the *trans* isomer is significantly easier to reduce. Accordingly, DFT calculations indicate that the character of the LUMO differs in *cis* and *trans* isomers. The d-orbital in the *trans* isomer LUMO is primarily σ-antibonding with axial chlorides, but in the *cis* isomer, the corresponding orbital is σ-antibonding with the chlorides as

well as the more strongly donating pincer nitrogen, which causes additional destabilization (Figure S31).

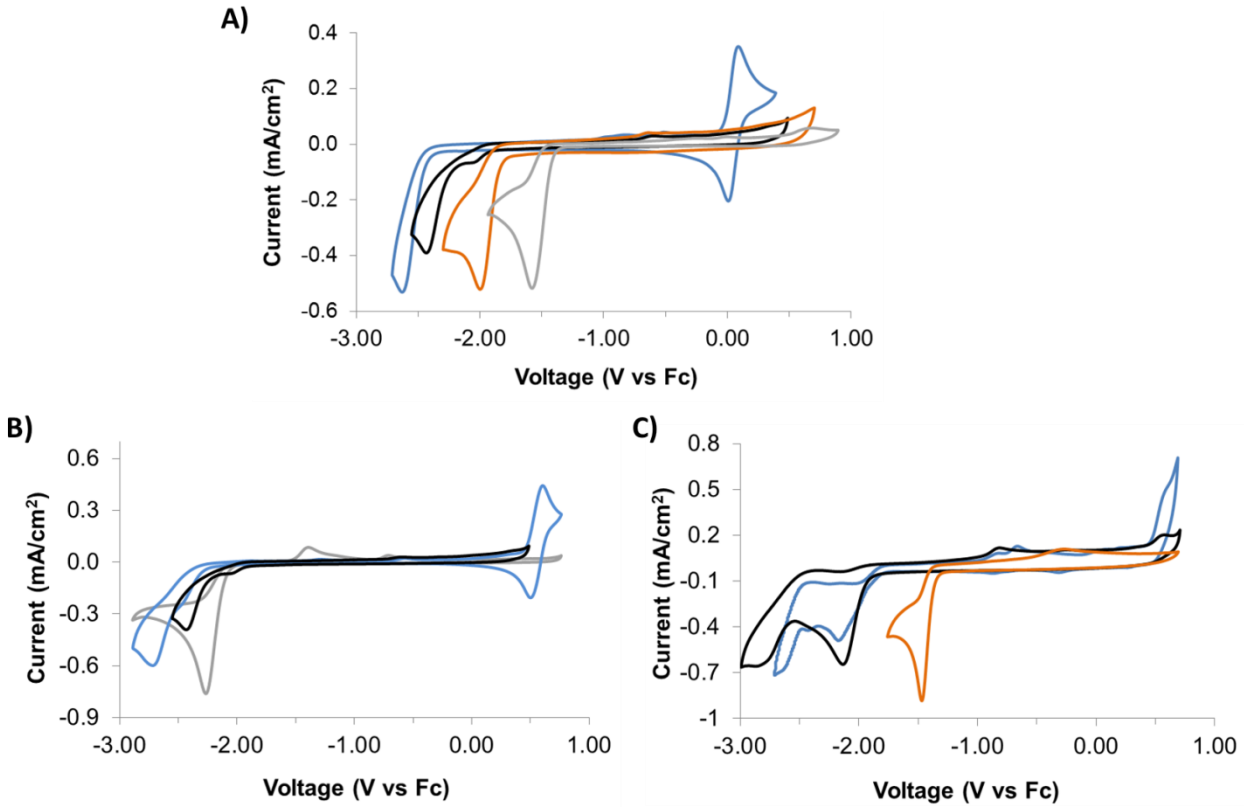

Figure 7. Cyclic voltammograms of selected pincer Ru complexes showing impacts of the following modifications: A) Monodentate ligand variation in $^{tBu}SN^{H}S$ complexes: **7-PPh$_3$** (blue), **7-CO** (black), **7-ACN** (orange), **7-2CO** (grey). (B) Heteroatom modification and methylation in aliphatic pincer complexes: *cis*-**8-CO** (blue), **7-CO** (black), **10-CO** (grey). (C) Monodentate ligand variation in $^{tBu}SN_{py}S$ complexes: **5-PPh$_3$** (blue), **5-CO** (black), **5-2CO** (orange). All voltammograms were collected under argon in 0.1M $TBAPF_6$/ACN at a scan rate of 100mV/s.

The impact of isomers on electrochemical properties complicates interpretation of the CV of **7-CO** where structural assignment is more difficult (*vide supra*). However, **7-CO** is clearly more easily reduced (-2.41 V) than either isomer of **8-CO** (-2.51 and -2.71 V). This suggests that regardless of the major isomer present, the $^{tBu}SN^{H}S$ Ru complex is less electron rich than its $PN^{H}P$ analogue owing to weaker donation from sulfur relative to phosphine. The magnitude of the impact of the heteroatom substitution is difficult to gauge and ranges from 0.1-0.3 V depending on the major isomer considered. Comparison of **7-CO** to **10-CO** (*cis* geometry) reveals a relatively anodic reduction for the ^{tBu}**SN^{Me}S** analogue (Figure 7B). The calculated

energies of the LUMOs agree with this relationship when using *cis* but not *trans* halide geometry for **7-CO**, perhaps indicating that *cis* is the major isomer (Figure S32). Meanwhile, optimized *cis* structures calculated for **7-CO** and **10-CO** show that even though ^{tBu}**SN^{Me}S** may seem more inductively donating, the enhanced sterics of N-Me versus N-H force a longer Ru-N bond (calcd. 2.21 vs 2.14 Å), weakening donation and possibly explaining the less cathodic reduction. Similar Ru-N bond elongation has previously been observed in PNP Ru carbonyl hydrides, [Ru(^{iPr}PN^{R}P)(CO)(H)(Cl)] (R = H, Me), where the metal-amine bond is 2.247(2)Å for methylated amine versus 2.195(2)Å for N-H.[10b]

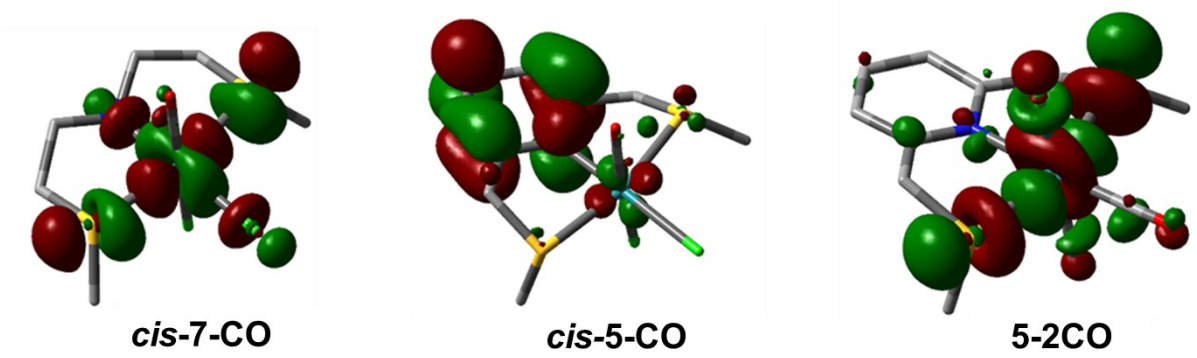

Figure 8. Illustration of ground state LUMOs calculated for SNS complexes. DFT computations were conducted using the B3LYP functional with a split basis set, LanL2DZ on Ru and 6-31+G** for all non-heavy atoms.

As with changes to the pincer ligand, replacing the monodentate ligands in **7-CO** effects reduction potential (Figure 7A). Exchanging the strong π acceptor CO for the strong σ-donor PPh_3 in **7-PPh$_3$** shifts reduction cathodically. Again though, the magnitude of the effect is difficult to judge since differences in the geometries of **7-CO** and **7-PPh$_3$** may also impact potential.[50] Exchanging a chloride ligand in **7-CO** for a neutral ACN ligand leads to an overall positive charge causing an anodic shift in reduction. Further anodic shifting results from swapping ACN for the strong π acid CO in **7-2CO**, and overall, monodentate ligand variations studied here tune the reduction potential of the aliphatic SNS architecture over a range of 1.05V. DFT calculations nicely predict the observed trends (Figure S33).

Relative to the aliphatic SNS Ru complexes, the reductions of the **^{tBu}SN$_{py}$S** Ru complexes **5-CO** and **5-PPh$_3$** are slightly less cathodic and exhibit dramatically different redox behavior (Figure 7C). Initial reduction in these complexes remains irreversible but is broadened, less stable to cycling, and significantly less responsive to changes in the identity of the

monodentate ligands (ΔE = -0.04V for **5-PPh$_3$** vs **5-CO**, ΔE = -0.22V for **7-PPh$_3$** vs **7-CO**). Calculations on **5-CO** offer a possible explanation for this difference by showing a LUMO where reduction no longer occurs mostly on the metal center but instead is dominated by the π-system of the chelate pyridine ring (Figure 8). This ligand centric reduction was experimentally confirmed by conducting voltammetry with [(^{tBu}SN$_{py}$S)ZnCl$_2$] which gives nearly the same reduction as **5-CO** and **5-PPh$_3$** despite having a redox inactive metal center (Figure S17). In addition to their ligand based reduction, **5-CO** and **5-PPh$_3$** also have a second irreversible reduction *ca* -2.8 V. This process more closely resembles the reductions of the aliphatic SNS family and thus likely shares their metal based nature. Finally, cationic **^{tBu}SN$_{py}$S** complex **5-2CO** exhibits a redox profile distinct from its neutral counterparts **5-CO** and **5-PPh$_3$**. The cation is significantly easier to reduce (-1.47V) owing to its overall charge and two π-acidic carbonyl ligands. Moreover, it undergoes only a single reduction which is sharper and more stable to cycling than the observed pyridine based processes. Consistent with this, the calculated LUMO for **5-2CO** resides largely on the metal with little pyridine character (Figure 8).

The prior success of SNS Ru complexes as thermal catalysts for CO_2 reduction and emerging reports of thiolate Co[51] and Mo[52] complexes as electrocatalysts for this process have motivated preliminary screening of the SNS complexes **5-CO**, **5-2CO**, **7-CO**, and **7-ACN** for electrocatalysis (See SI for complete details). During cyclic voltammetry in ACN, all of the complexes except **5-2CO** show significant enhancement of their reductive response under CO_2 with further enhancement occuring upon addition of the proton source trifluoroethanol (TFE). Unfortunately, electrolysis experiments in the presence of CO_2 and TFE show that reductive currents generated by the SNS complexes either fall off quickly over time or are maintained but lead only to minimal production of CO_2 derived products, such as CO and formate.

Implications for (De)Hydrogenation Catalysis

Insight from the electrochemical characterization adds perspective to discussions on (de)hydrogenative catalysis with pincer complexes. Based on comparisons of reduction in **8-CO** and **7-CO**, swapping SNS for PNP can lower the electron density at the metal center, but geometric disparities can attenuate this effect. In the frequent comparisons of PN^{H}P carbonyl complex **1** to **6**, competing electronic effects caused by simultaneously changing the pincer (PNP vs SNS) and monodentate ligand (CO vs PPh_3) likely offset, as seen in *trans*-**8-CO** vs **7-PPh$_3$**. Therefore, other effects such as reduced sterics and increased hemilability in the SNS catalyst

may be significant in explaining the improved activity of SNS catalysts in some transfer[20a] and ester hydrogenation[18a,25] reactions. Additionally, electronic effects cannot be discounted in the improvement of ester hydrogenation catalysis observed with **7-PPh$_3$** as compared to less electron rich **7-CO**.[18a] The higher electron density observed for the former should facilitate ester insertion into an active metal hydride, a key step in the catalytic mechanism.[23] Differences in electronic structure may also impact performance of methylated pincer complexes. A pronounced decrease in electron density in **10-CO** has been observed relative to **7-CO** and appears to be a general effect also occurring in Fe PNP complexes. Preliminary CV experiments comparing N-Me and N-H versions of [Fe(^{iPr}PN^{R}P)(CO)$_2$H](OTf) (R = H and Me) and [Fe(^{iPr}PN^{R}P)(HCOO)(CO)H] (R = H and Me) indicate the N-Me variants undergo more mild reductions by *ca* 0.10 to 0.15V (See SI). Of course, these changes in electron density must be considered in context with the other critical impacts of pincer methylation such as loss of metal-ligand cooperativity and preclusion of hydrogen bonding.[10b,53]

The SNS dicarbonyl complex **7-2CO** prepared here allows for comparison to PNP dicarbonyl **8-2CO** which is closely related to a key deactivated species in PNP Ru catalysis. The shortened C-O bond lengths in the SNS derivative **7-2CO** relative to PNP complex **8-2CO** indicate less backbonding and lower metal electron density in the SNS complex. IR spectra further corroborate this by showing a significantly higher average CO stretching frequency for **7-2CO** (2040 cm^{-1} vs 2000 cm^{-1}).[44] The diminished backbonding in the SNS dicarbonyl may lead to a more labile CO ligand and reduce accumulation of the deactivated dicarbonyl species with SNS catalysts.

Conclusion

A series of Ru(II) SNS complexes with carbonyl ligands was prepared and characterized to probe structural and electrochemical trends associated with changes to the ancillary ligands especially the pincer ligands. Understanding the properties of these complexes is important because it may be possible to use SNS supported catalysts as air-stable and less electron rich versions of the Ru PN^{H}P pincer complexes used extensively in (de)hydrogenation reactions. However, comparison of Ru carbonyl complexes supported with SNS and PNP ligands, indicates that there are major differences in the properties of complexes with the two ligands. Synthetically, SNS ligands are less tolerant of silver reagents and less able to displace PPh$_3$ from common Ru sources as compared to PN^{H}P. In terms of structure, SNS complexes require

consideration of a wider array of geometric possibilities owing to variability in sulfur substituent positioning. Moreover, SNS Ru dichloride complexes tend to favor *cis* halide arrangement in contrast to the prevalence of *trans* isomers in PNP chemistry. Electrochemical and IR comparison shows that the SNS motif generally leads to less electron rich complexes than PNP, but this effect can be attenuated by variation in other supporting ligands and even geometric differences between structures. The type of SNS pincer backbone also significantly impacts redox properties with the methylated $^{tBu}SN^{Me}S$ ligands resulting in more facile reduction than $^{tBu}SN^{H}S$ ligands and pyridyl $^{tBu}SN_{py}S$ ligands resulting in ligand based reduction. Tailoring SNS complexes to replace PNP catalysts or to target catalysis with specific redox profiles will ultimately require careful selection of the pincer backbone, surrounding ligands, and even complex geometry.

Acknowledgements

The authors acknowledge support from the U.S. Department of Energy, Office of Science, Basic Energy Sciences, Catalysis Science Program, under Award DE-SC0018222. The computation for this work was performed on the high performance computing infrastructure provided by Research Computing Support Services and in part by the National Science Foundation under grant number CNS-1429294 at the University of Missouri, Columbia MO.

Supporting information

Additional information about experimental details and characterization data, NMR spectra, electrochemical data, X-ray diffraction information (CCDC: 2105455-2105459, 2118216) and computational details are available via the Internet.

Competing Financial Interests

The authors declare no competing financial interests.

References

[1] Gunanathan, C.; Milstein, D. Bond Activation and Catalysis by Ruthenium Pincer Complexes. *Chem. Rev.* **2014**, *114*(24), 12024-12087.

[2] (a) Werkmeister, S.; Neumann, J.; Junge, K.; Beller, M. Pincer-Type Complexes for Catalytic (De)Hydrogenation and Transfer (De)Hydrogenation Reactions: Recent Progress. *Chem. Eur. J.* **2015**, *21*(35), 12226-12250. (b) Younus, H.A.; Su, W.; Ahmad, N.; Chen, S.; Verpoort, F. Ruthenium Pincer Complexes: Synthesis and Catalytic Applications. *Adv. Synth. Catal.* **2015,** *357*, 283-330.

[3] Nielsen, M.; Alberico, E.; Baumann, W.; Drexler, H.-J.; Junge, H.; Gladiali, S.; Beller, M. Low-temperature Aqueous-phase Methanol Dehydrogenation to Hydrogen and Carbon Dioxide *Nature*. **2013**, *495*, 85–89.
[4] Nielsen, M.; Junge, H.; Kammer, A.; Beller, M. Towards a Green Process for Bulk-Scale Synthesis of Ethyl Acetate: Efficient Acceptorless Dehydrogenation of Ethanol. *Angew. Chem. Int. Ed.* **2012**, *51*(23), 5711-5713.
[5] (a) Rezayee, N.M.; Huff, C.A.; Sanford, M.S. Tandem Amine and Ruthenium-Catalyzed Hydrogenation of CO2 to Methanol. *J. Am. Chem. Soc.* **2015**, *137*, 1028-1031. (b) Kothandaraman, J.; Goeppert, A.; Czaun, M.; Olah, G.A.; Prakash, G.K.S. Conversion of CO_2 from Air into Methanol Using a Polyamine and a Homogeneous Ruthenium Catalyst. *J. Am. Chem. Soc.* **2016**, *138*, 778-781. (c) Sen, R.; Goeppert, A.; Kar, S.; Prakash, G.K.S. Hydroxide Based Integrated CO_2 Capture from Air and Conversion to Methanol. *J. Am. Chem. Soc.* **2020**, *142*(10), 4544-4549.
[6] Kuriyama, W.; Matsumoto, T.; Ogata, O.; Ino, Y.; Aoki, K.; Tanaka, S.; Ishida, K.; Kobayashi, T.; Sayo, N.; Saito, T. Catalytic Hydrogenation of Esters. Development of an Efficient Catalyst and Processes for Synthesising (R)-1,2-Propanediol and 2-(l-Menthoxy)ethanol. *Org. Process Res. Dev.* **2012**, *16*, 166-171.
[7] Filonenko, G.A.; van Putten, R.; Schulpen, E.N.; Hensen, E.J.M.; Pidko, E.A. Highly Efficient Reversible Hydrogenation of Carbon Dioxide to Formates Using a Ruthenium PNP-Pincer Catalyst. *ChemCatChem.* **2014**, *6*(6), 1526-1530.
[8] (a) Balaraman, E.; Gnanaprakasam, B.; Shimon, L.J.W.; Milstein, D. Direct Hydrogenation of Amides to Alcohols and Amines under Mild Conditions. *J. Am. Chem. Soc.* **2010**, *132*(47), 16756-16758. (b) Mukherjee, A.; Srimani, D.; Ben-David, Y.; Milstein, D. Low-Pressure Hydrogenation of Nitriles to Primary Amines Catalyzed by Ruthenium Pincer Complexes. Scope and mechanism. *ChemCatChem.* **2017**, *9*(4), 559-563.
[9] (a) Li, H.; Hall, M.B. Computational Mechanistic Studies on Reactions of Transition Metal Complexes with Noninnocent Pincer Ligands: Aromatization–Dearomatization or Not. *ACS Catal.* **2015**, *5*(3), 1895-1913. (b) Mathis, C.L.; Geary, J.; Ardon, Y.; Reese, M.S.; Philliber, M.A.; VanderLinden, R.T.; Saouma, C.T. Thermodynamic Analysis of Metal–Ligand Cooperativity of PNP Ru Complexes: Implications for CO_2 Hydrogenation to Methanol and Catalyst Inhibition. *J. Am. Chem. Soc.* **2019**, *141*(36), 14317-14328.
[10] (a) Yang, X. Mechanistic Insights into Ruthenium-Catalyzed Production of H_2 and CO_2 from Methanol and Water: A DFT Study. *ACS Catal.* **2014**, *4*(4), 1129-1133. (b) Alberico, E.; Lennox, A.J.J.; Vogt, L.K.; Jiao, H.; Baumann, W.; Drexler, H.-J.; Nielsen, M.; Spannenberg, A.; Checinski, M.P.; Junge, H.; Beller, M. Unravelling the Mechanism of Basic Aqueous Methanol Dehydrogenation Catalyzed by Ru–PNP Pincer Complexes. *J. Am. Chem. Soc.* **2016**, *138*(45), 14890-14904. (c) Nguyen, D.H.; Trivelli, X.; Capet, F.; Swesi, Y.; Favre-Réguillon, A.; Vanoye, L.; Dumeignil, F.; Gauvin, R.M. Deeper Mechanistic Insight into Ru Pincer-Mediated Acceptorless Dehydrogenative Coupling of Alcohols: Exchanges, Intermediates, and Deactivation Species. *ACS Catal.* **2018**, *8*(5), 4719-4734. (d) Sinha, V.; Govindarajan, N.; de Bruin, B.; Meijer, E. J. How Solvent Affects C–H Activation and Hydrogen Production Pathways in Homogeneous Ru-Catalyzed Methanol Dehydrogenation Reactions. *ACS Catal.* **2018**, *8*(8), 6908-6913.

[11] Kar, S.; Sen, R.; Kothandaraman, J.; Goeppert, A.; Chowdhury, R.; Munoz, S.B.; Haiges, R.; Prakash, G.K.S. Mechanistic Insights into Ruthenium-Pincer-Catalyzed Amine-Assisted Homogeneous Hydrogenation of CO_2 to Methanol. *J. Am. Chem. Soc.* **2019**, *141*(7), 3160-3170.
[12] (a) Das, U. K.; Daifuku, S. L.; Iannuzzi, T. E.; Gorelsky, S. I.; Korobkov, I.; Gabidullin, B.; Neidig, M. L.; Baker, R. T. Iron(II) Complexes of a Hemilabile SNS Amido Ligand: Synthesis, Characterization, and Reactivity. *Inorg. Chem*. **2017**, *56*(22), 13766–13776. (b) Elsby, M. R.; Ghostine, K.; Das, U. K.; Gabidullin, B. M.; Baker, R. T. Iron-SNS and -CNS Complexes: Selective C_{aryl}–S Bond Cleavage and Amine-Borane Dehydrogenation Catalysis. *Organometallics.* **2019**, *38* (19), 3844-3851. (c) Elsby, M. R.; Baker, R. T. Cu(I)–SNS Complexes for Outer-sphere Hydroboration and Hydrosilylation of Carbonyls *Chem. Commun*. **2019**, *55*, 13574-13577.
[13] (a) Sogukomerogullari, H.G.; Aytar, E.; Ulusoy, M.; Demir, S.; Dege, N.; Richeson, D.S.; Sönmez, M. Synthesis of Complexes Fe, Co and Cu Supported by "SNS" Pincer Ligands and Their Ability to Catalytically Form Cyclic Carbonates. *Inorganica Chim. Acta.* **2018**, *471*, 290-296. (b) Soobramoney, L.; Bala, M.D.; Friedrich, H.B.; Pillay, M.N. Flexible SNS Pincer Complexes of Copper: Synthesis, Structural Characterisation and Application in n-Octane Oxidation. *Polyhedron,* **2019**, *163*(1), 63-70.
[14] (a) Fiebor, A.; Tia, R.; Makhubela, B.C.E.; Kinfe, H.H. Water-soluble SNS Cationic Palladium(II) Complexes and Their Suzuki–Miyaura Cross-coupling Reactions in Aqueous Medium. *Beilstein J. Org. Chem.* **2018,** *14,* 1859–1870. (b) Flores-Rojas, G.G.; González-Sebastián, L.; Reyes-Martínez, R.; Aguilar-Castillo, B.A.; Hernández-Ortega, S.; Morales-Morales, D. Synthesis and Characterization of Pd(II) Complexes Bearing NS, CS, SNS and SCS ligands. Evaluation of their Microwave Assisted Catalytic Activity in C-C Coupling Reactions. *Polyhedron*. **2020**, *185*(15), 114601.
[15] (a) Bai, S.-Q.; Hor, T.S.A. Isolation of an [SNS]Pd(II) Pincer with a Water Ladder and its Suzuki Coupling Activity in Water. *Chem. Commun.* **2008**, *27*, 3172-3174. (b) Kumar, S.; Rao, G. K.; Kumar, A.; Singh, M. P.; Singh, A.K. Palladium(II)-(E,N,E) Pincer Ligand (E = S/Se/Te) Complex Catalyzed Suzuki Coupling Reactions in Water via In-situ Generated Palladium Quantum Dots. *Dalton Trans.* **2013**, *42*(48), 16939-16948.
[16] (a) McGuinness, D.S.; Wasserscheid, P.; Keim, W.; Morgan, D.; Dixon, J.T.; Bollmann, A.; Maumela, H.; Hess, F.; Englert, U. First Cr(III)−SNS Complexes and Their Use as Highly Efficient Catalysts for the Trimerization of Ethylene to 1-Hexene. *J. Am. Chem. Soc.* **2003**, *125*(18), 5272-5273. (b) McGuinness, D.S.; Brown, D.B.; Tooze, R.P.; Hess, F.M.; Dixon, J.T.; Slawin, A.M.Z. Ethylene Trimerization with Cr−PNP and Cr−SNS Complexes: Effect of Ligand Structure, Metal Oxidation State, and Role of Activator on Catalysis. *Organometallics.* **2006**, *25*, 3605-3610. (c) Dixon, J.T.; Wasserscheid, P.; Mcguinness, D.S.; Hess, F.M.; Maumela, H.; Morgan, D.H.; Bollmann, A. "Trimerisation and oligomerisation of olefins using a chromium based catalyst." WIPO patent WO2003053890A1, July 3, 2003.
[17] Page, M.J.; Wagler, J.; Messerle, B.A. Pyridine-2,6-bis(thioether) (SNS) Complexes of Ruthenium as Catalysts for Transfer Hydrogenation. *Organometallics.* **2010**, *29*, 3790-3798.
[18] (a) Spasyuk, D.; Smith, S.; Gusev, D.G. Replacing Phosphorus with Sulfur for the Efficient Hydrogenation of Esters. *Angew. Chem.* **2013**, *125*, 2598-2602. (b) Vicent, C.; Gusev, D.G. ESI-MS Insights into Acceptorless Dehydrogenative Coupling of Alcohols. *ACS Catal.* **2016**, *6*, 3301-3309.

[19] Zhang, L.; Han, Z.; Zhao, X.; Wang, Z.; Ding, K. Highly Efficient Ruthenium-Catalyzed N-Formylation of Amines with H_2 and CO_2. *Angew. Chem.* **2015**, *127*(21), 6284-6287.
[20] (a) Dubey, A.; Khaskin, E. Catalytic Ester Metathesis Reaction and Its Application to Transfer Hydrogenation of Esters. *ACS Catal.* **2016**, *6*(6), 3998-4002. (b) Jankins, T.C.; Fayzullin, R.R.; Khaskin, E. Three-Component [1 + 1 + 1] Cyclopropanation with Ruthenium(II). *Organometallics* **2018**, *37*(15), 2609-2617.
[21] Hinzmann, A.; Gröger, H. Selective Hydrogenation of Fatty Nitriles to Primary Fatty Amines: Catalyst Evaluation and Optimization Starting from Octanenitrile. *Eur. J. Lipid Sci. Technol.* **2020**, *122*, 1900163.
[22] Waldie, K.M.; Ostericher, A.L.; Reineke, M.H.; Sasayama, A.F.; Kubiak, C.P. Hydricity of Transition-Metal Hydrides: Thermodynamic Considerations for CO_2 Reduction. *ACS Catal.* **2018**, *8*(2), 1313-1324.
[23] For a recent discussion on the effects of ligand electron donation on elementary (de)hydrogenation steps, see: Liu, H.; Wang, W.-H.; Xiong, H.; Nijamudheen, A.; Ertem, M.Z.; Wang, M.; Duan, L. Efficient Iridium Catalysts for Formic Acid Dehydrogenation: Investigating the Electronic Effect on the Elementary β-Hydride Elimination and Hydrogen Formation Steps. *Inorg. Chem.* **2021**, *60*, 3410-3417.
[24] (a) Viñas, C. *et al.* Ruthenium(II) Complexes with NS2 Pyridine-Based Dithia-Containing Ligands. Proposed Possible Structural Isomers and X-ray Confirmation of Their Existence. *Inorg. Chem.* **1998**, *37*(4), 701-707. (b) Teixidor, F.; Anglès, P.; Viñas, C.; Kivekäs, R.; Sillanpää, R. Comparative Study of NS_2(S-aryl) Pyridine-Based Dithia-Containing Ligands with Different Substituent Groups. Reactivity toward Cu(II) and Ru(II). *Inorg. Chem.* **2001**, *40*(16), 4010-4015.
[25] Schörgenhumer, J.; Zimmermann, A.; Waser, M. SNS-Ligands for Ru-Catalyzed Homogeneous Hydrogenation and Dehydrogenation Reactions. *Org. Process Res. Dev.* **2018**, *22*, 862-870.
[26] Spasyuk, D.; Gusev, D. G. Acceptorless Dehydrogenative Coupling of Ethanol and Hydrogenation of Esters and Imines. *Organometallic* **2012**, *31*(15), 5239-5242.
[27] ^{tBu}**SN^{H}S** and [Ru(CO)(DMF)(PPh_3)$_2$(Cl)$_2$] were heated up to 92ºC in dioxane for ~5 hours.
[28] Ziessel, R.; Grosshenny, V.; Hissler, M.; Stroh, C. *cis*-[Ru(2,2‘:6‘,2‘ ‘-terpyridine)(DMSO)Cl_2]: Useful Precursor for the Synthesis of Heteroleptic Terpyridine Complexes under Mild Conditions. *Inorg. Chem.* **2004**, *43*(14), 4262-4271.
[29] For more examples of neutral ruthenium complexes with DMSO and their NMR shifts see: (a) Tan, C.; Hu, S.; Liu, J.; Ji, L. Synthesis, Characterization, Antiproliferative and Anti-metastatic Properties of Two Ruthenium–DMSO Complexes Containing 2,2′-biimidazole. *Eur. J. Med. Chem.* **2011**, *46*, 1555-1563. (b) Roeser, S.; Maji, S.; Benet-Buchholz, J.; Pons, J.; Llobet, A. Synthesis, Characterization, Reactivity, and Linkage Isomerization of $Ru(Cl)_2(L)(DMSO)_2$ Complexes. *Eur. J. Inorg. Chem.* **2013**, 232-240. (c) Leung, C.-F.; Wong, C.-Y.; Ko, C.-C.; Yuen, M.-C.; Wong, W.-T.; Wong, W.-Y.; Lau, T.-C. 8-Quinolinolato Complexes of Ruthenium(II) and (III). *Inorganica Chim. Acta.* **2009**, *362*(4), 1149-1157.
[30] (a) Root, M.J.; Deutsch, E. Synthesis and Characterization of (Bipyridine)(terpyridine) (chalcogenoether)ruthenium(II) Complexes. Kinetics and Mechanism of the Hydrogen Peroxide Oxidation of $[(bpy)(tpy)RuS(CH_3)_2]^{2+}$ to $[(bpy)(tpy)RuS(0)(CH_3)_2]^{2+}$. Kinetics of the Aquation of $[(bpy)(tpy)RuS(0)(CH_3)_2]^{2+}$. *Inorg. Chem.* **1985**, *24*, 1464-1471. (b) Smith, M.K.; Gibson, J.A.; Young, C.G.; Broomhead, J.A.;

Junk, P.C.; Keene, F.R. Photoinduced Ligand Isomerization in Dimethyl Sulfoxide Complexes of Ruthenium(II). *Eur. J. Inorg. Chem.* **2000**, 1365-1370.
[31] Calligaris, M. Structure and Bonding in Metal Sulfoxide Complexes: an Update. *Coord. Chem. Rev.* **2004**, *248*, 351-375.
[32] Gibson, D.H.; Pariya, C.; Mashuta, M.S. Synthesis and Characterization of Ruthenium(II) Hydrido and Hydroxo Complexes Bearing the 2,6-Bis(di-tert-butylphosphinomethyl)pyridine Ligand. *Organometallics* **2004**, *23*(10), 2510-2513.
[33] See SI in: Stewart, D.J.; Fanwick, P.E.; McMillin, D.R. A Red-Emitting Light Switch Based on a Heteroleptic Ruthenium(II) Complex Containing a Tridentate dppz Analogue. *Inorg. Chem.* **2010**, *49*(15), 6814-6816.
[34] Mixing **7-CO** and $AgPF_6$ under CO atmosphere leads to consumption of starting material and production of a complicated, new ^{1}H NMR spectrum. However, this same spectrum can also be generated in control reactions without CO and thus does not indicate the desired addition of CO to **7-CO**. The consumption of **7-CO** may involve some reaction with the silver alone, but participation by the acetone solvent required for solubility cannot be ruled out.
[35] Replacement of Cl with ACN was also attempted using $AgPF_6$ as the abstraction agent, but again, the addition of Ag proved problematic giving a product with a multitude of NMR signals. Similar installation of ACN using Ag reagents has proceeded smoothly in some bulky SNS complexes in ref 17, but that reference also describes formation of Ag bridged dimers in less bulky complexes. Thus, although Ag is widely employed for abstraction in PNP chemistry, it is clearly less tolerated in the synthesis of SNS Ru complexes.
[36] The ^{1}H NMR signal for ruthenium bound ACN varies widely depending on the overall charge of the complex and the ligand trans to the ACN but many appear between ~1.9 – 2.9 ppm based on ref. 17 and: Sharma, R.; Knoll, J.D.; Ancona, N.; Martin, P.D.; Turro, C.; Kodanko, J.J. Solid-Phase Synthesis as a Platform for the Discovery of New Ruthenium Complexes for Efficient Release of Photocaged Ligands with Visible Light. *Inorg. Chem.* **2015**, *54*(4), 1901-1911.
[37] Intramolecular hydrogen bonding between the secondary amine in SNS and bound chloride has previously been observed in a chromium complex (2.71Å, ref. 16b) while hydrogen bonding to outersphere chloride counterions has also been observed in Pd SNS complexes (3.14Å, ref. **Error! Bookmark not defined.**a). By comparison, such interactions are not generally noted in P NP structures including the crystal structure presented here for complex **8-CO**.
[38] (a) Rachford, A.A.; Petersen, J.L.; Rack, J.J. Designing Molecular Bistability in Ruthenium Dimethyl Sulfoxide Complexes. *Inorg. Chem.* **2005**, *44*(22), 8065-8075. (b) Rachford, A.A.; Petersen, J.L.; Rack, J.J. Efficient Energy Conversion in Photochromic Ruthenium DMSO Complexes. *Inorg. Chem.* **2006**, *45*(15), 5953-5960. (c) Ferrer, Í.; Fontrodona, X.; Rodríguez, M.; Romero, I. Ru(II)-dmso Complexes Containing Azole-based Ligands: Synthesis, Linkage Isomerism and Catalytic Behaviour. *Dalton Trans.* **2016**, *45*, 3163-3174.
[39] The small difference in calculated energy between *fac* and *mer* isomers for **7-DMSO** means that a mixture of isomers should be thermodynamically allowed. Thus, the observation of one compound by NMR spectroscopy is due to a kinetic barrier to interconversion (not calculated here).
[40] Crystallization produces pure *trans*-**8-CO** but recovered *cis*-**8-CO** is always contaminated with varying amounts of the *trans* isomer. Crystals suitable for diffraction could not be grown for *cis*-**8-CO**, but its identity is verified based on the literature precedent in ref 26 as well as its ^{1}H NMR and IR spectra and elemental analysis, which show the necessary similarity to *trans*-**8-CO**.

[41] For examples of [Ru(^{R}PNP)(CO)(H)(Cl)] complexes see ref.10b. For a dichloro carbonyl PNP structure see: Krishnakumar, V.; Chatterjee, B.; Gunanathan, C. Ruthenium-Catalyzed Urea Synthesis by N–H Activation of Amines. *Inorg. Chem.* **2017**, *56*(12), 7278-7284. For examples of structures with the form [Ru(^{R}PNP)(PPh_3)($Cl)_2$] see: Rahman, M.S.; Prince, P.D.; Steed, J.W.; Hii, K.K. Coordination Chemistry and Catalytic Activity of Ruthenium Complexes of Terdentate Phosphorus−Nitrogen−Phosphorus (PNP) and Bidentate Phosphorus−Nitrogen (PNH) Ligands. *Organometallics.* **2002**, *21*, 4927-4933.

[42] The CO bond length in the crystal structure of **8-CO** suffers data abnormalities, so the CO lengths for **8-CO** and **10-CO** cannot be directly compared to further establish the enhanced backbonding in PNP structures. However, the CO length in **10-CO** (1.143(3)Å) is shorter as compared to the range of CO lengths (1.15-1.158Å) found in published structures of popular [Ru(^{R}PNP)(H)(CO)(Cl)] complexes (ref. 10b) and [Ru(^{Ph}PNP)(CO)($Cl)_2$] complexes in the following references: (a) Bianchini, C.; Innocenti, P.; Peruzzini, M.; Romerosa, A.; Zanobini, F. C−C Bond Formation between Vinylidene and Alkynyl Ligands at Ruthenium(II) Leading to either Enynyl or Dienynyl Complexes. *Organometallics.* **1996**, *15*, 272-285. (b) Zhang, L. *et al.* Acceptorless Dehydrogenative Coupling of Alcohols Catalysed by Ruthenium PNP Complexes: Influence of Catalyst Structure and of Hydrogen Mass Transfer. *J. Catal.* **2016**, *340*, 331-343.

[43] Poor solubility prevented crystallization of **7-CO** whereas crystals were obtained for **7-ACN** but were seemingly too dependent on solvent intercalation to survive transfer to the X-ray diffractometer.

[44] Rozenel, S.S.; Arnold, J. Bimetallic Ruthenium PNP Pincer Complex As a Platform to Model Proposed Intermediates in Dinitrogen Reduction to Ammonia. *Inorg. Chem.* **2012**, *51*, 9730-9739.

[45] Reduction remains irreversible even if scan rate is increased from 100mV/s to 450mV/s. In addition to the major reduction, a very small reduction is observed for **7-CO** near -2.2V. This could represent a minute contaminate, but because multiple isomers are suggested via spectroscopy, it more likely indicates a minor isomer.

[46] It is expected that S-^{t}Bu orientation isomers will not be distinct in CV experiments as these changes will have little/no impact on the energies of the frontier molecular orbitals.

[47] (a) Caemelbecke, E.V.; Kutner, W.; Kadish, K.M. Electrochemical and Spectroelectrochemical Characterization of (5,10,15,20-Tetrakis(l-methyl-4-pyridyl)porphinato)manganese(III) Chloride, [(TMpyP)$Mn^{III}Cl]^{4+}(Cl^{-})_4$, in N,N-Dimethylformamide. *Inorg. Chem.* **1993**, *32*, 438-444. (b) Lindley, B.M.; van Alten, R.S.; Finger, M.; Schendzielorz, F.; Würtle, C.; Miller, A.J.M.; Siewert, I.; Schneider, S. Mechanism of Chemical and Electrochemical N_2 Splitting by a Rhenium Pincer Complex. *J. Am. Chem. Soc.* **2018**, *140*, 7922-7935. (c) Chirdon, D.N.; Transue, W.J.; Kagalwala, H.N.; Kaur, A.; Maurer, A.B.; Pintauer, T.; Bernhard, S. [Ir(N^N^N)(C^N)L]+: A New Family of Luminophores Combining Tunability and Enhanced Photostability. *Inorg. Chem.* **2014**, *53*, 1487-1499.

[48] Because the LUMO includes an antibonding interaction between the metal and the pincer sulfur donors, dissociation of a sulfur upon reduction could also explain the observed behavior, but dissociation is exepected to be reversible due to chelation effects.

[49] (a) Lever, A.B.P. Electrochemical Parametrization of Metal Complex Redox Potentials, Using the Ruthenium(III)/Ruthenium(II) Couple To Generate a Ligand Electrochemical Series. *Inorg. Chem.* **1990**, *29*, 1271-1285. (b) Sullivan, B.P.; Calvert, J.M.; Meyer, T.J. Cis-Trans Isomerism in (trpy) (PPh_3)$RuCl_2$. Comparisons between the Chemical and Physical Properties of a

Cis-Trans Isomeric Pair. *Inorg. Chem.* **1980**, *19*(5), 1404-1407. (c) Nakamura, G.; Okamura, M.; Yoshida, M.; Suzuki, T.; Takagi, H.D.; Kondo, M.; Masaoka, S. Electrochemical Behavior of Phosphine-Substituted Ruthenium(II) Polypyridine Complexes with a Single Labile Ligand. *Inorg. Chem.* **2014**, *53* (14), 7214-7226.

[50] Whereas **7-CO** is proposed to exist as the *cis* isomer, **7-PPh$_3$** could adopt a *trans* geometry like its $^{Et}SN^{H}S$ analogue (ref 18a) or it may feature *cis* halide coordination to allow for the bulky PPh_3 and S-^{t}Bu groups to be anti. If **7-PPh$_3$** were to adopt the more easily reduced *trans* configuration and **7-CO** were *cis*, this geometric disparity would undercut cathodic shifting by PPh_3.

[51] (a) Dey, S.; Ahmed, M.E.; Dey, A. Activation of Co(I) State in a Cobalt-Dithiolato Catalyst for Selective and Efficient CO_2 Reduction to CO. *Inorg. Chem.* **2018**, *57*(10), 5939-5947. (b) Dey, S.; Todorova, T.K.; Fontecave, M.; Mougel, V. Electroreduction of CO_2 to Formate with Low Overpotential using Cobalt Pyridine Thiolate Complexes. *Angew. Chem. Int. Ed.* **2020**, *59*(36), 15726-15733.

[52] Mouchfiq, A.; Todorova, T.K.; Dey, S.; Fontecave, M.; Mougel, V. A Bioinspired Molybdenum–copper Molecular Catalyst for CO_2 Electroreduction. *Chem. Sci.* **2020**, *11*, 5503-5510.

[53] Zhang, Y.; MacIntosh, A.D.; Wong, J.L.; Bielinski, E.A.; Williard, P.G.; Mercado, B.Q.; Hazari, N.; Bernskoetter, W.H. *Chem. Sci.* **2015**, *6*, 4291.

For Table of Contents Use Only